

## Supplementary Information

### Methods

#### Large indentation of incompressible neo-Hookean material

Hertz equation has been widely used to determine the Young's modulus of elastic materials when a semi-infinite half space of the materials is indented by an AFM probe. Its derivation assumes the indentation to be small, i.e.,  $\beta < 0.1$ , where  $\beta = \delta/R$ ,  $\delta$  is the indentation depth, and  $R$  is the tip radius of AFM probe. For analysis of very soft materials/tissues, the assumption may not be satisfied because the deformation has to be adequately large in order for the indentation force to be larger than the detection limit of AFM. To this end, we developed a new approach to determining the Young's modulus of TM. It was modified from those described in the literature,<sup>1-4</sup> where the indentation of the semi-infinite half space was modeled as one-dimensional (1-D) compression of a cylinder. For neo-Hookean materials, the normal Cauchy stress ( $\sigma$ ) for compression was a nonlinear function of extension ratio ( $\lambda$ ),

$$\sigma = B_1(\lambda^2 - \lambda^{-1}) \quad (S1)$$

where  $B_1$  is a material constant,  $\sigma = -F/\pi a^2$ ,  $F$  is the indentation force on the AFM probe, and  $a$  is the cylinder radius that is assumed to be the same as the radius of contact area. Dimensional analysis for the indentation of semi-infinite half space yields,

$$\lambda = g\left(\frac{a}{R}\right) = 1 + b_1\frac{a}{R} + b_2\frac{a^2}{R^2} + O\left(\frac{a^3}{R^3}\right) \quad (S2)$$

$$\frac{a}{R} = f(x) = k_1x + k_2x^2 + O(x^3) \quad \text{where } x = \left(\frac{\delta}{R}\right)^{\frac{1}{2}} \quad (S3)$$

where  $b_i$  and  $k_i$  ( $i = 1, 2, 3, \dots$ ) are constants. It has been shown that  $(a/R)^2 = \delta/R$  when  $a$  is much less than  $R$ .<sup>5</sup> Thus,  $k_1 = 1$ . Substituting Equations S2 and S3 into Equation S1, and neglecting the terms higher than the second order, we obtained,

$$-F = 3\pi B_1 b_1 R^2 \left(\frac{\delta}{R}\right)^{\frac{3}{2}} \left[1 + \theta \left(\frac{\delta}{R}\right)^{\frac{1}{2}}\right] \quad \text{where } \theta = \frac{b_2}{b_1} \quad (S4)$$

When  $\delta/R \rightarrow 0$ ,

$$-F \rightarrow B_1 3b_1 \pi R^2 \left(\frac{\delta}{R}\right)^{\frac{3}{2}} = B_1 3b_1 \pi R^{\frac{1}{2}} \delta^{\frac{3}{2}} \quad (S5)$$

and Equations S2 should be consistent with the Hertz equation (i.e., Equation 1). As a result,

$$B_1 b_1 = -\frac{4E_0}{9\pi(1-\nu^2)} \quad (S6)$$

where  $E_0$  is the initial Young's modulus of neo-Hookean materials and  $\nu$  is the Poisson's ratio. Substituting Equation S6 into Equation S4 yields,

$$F = \frac{4E_0}{3(1-\nu^2)} R^2 \left(\frac{\delta}{R}\right)^{\frac{3}{2}} \left[1 + \theta \left(\frac{\delta}{R}\right)^{\frac{1}{2}}\right] \quad (S7)$$

which is also called **Equation 2** in the paper.

Ocular tissues are neither homogeneous, nor semi-infinite in size. Thus, data analysis with Equation S7 (or Equation 2) could only provide the apparent initial Young's modulus  $(E_0)_{app}$ . To determine the difference between  $(E_0)_{app}$  and  $E_0$ , we performed numerical simulations of tissue indentation, i.e., *in silico* AFM experiment. Results from the simulation showed that the difference was negligible, compared to the variation in  $E_0$  within a TM.

### Numerical simulations of tissue indentation

We performed three-dimensional numerical simulations of tissue indentation with an AFM probe. In all simulations, ocular tissues were assumed to be neo-Hookean materials, whose strain energy density function  $W$  was given by,

$$W = C_1(I_1 - 3) + D_1(J - 1)^2 \quad (S8)$$

where  $C_1$  and  $D_1$  are material constants,  $J$  is the determinant of the elastic deformation gradient,

$I_1 = I_1 J^{-\frac{2}{3}}$ , and  $I_1$  is the first invariant of the left Cauchy-Green deformation tensor. The material constant  $D_1$  is related the initial Young's modulus and Poisson's ratio by  $D_1 = E_0/[6(1-2\nu)]$ .

Tissue indentation in AFM experiments has been shown to be several orders of magnitude faster than water diffusion in the contact area.<sup>3</sup> In this regard, tissues can be treated as incompressible materials, which requires  $\nu$  to be 0.5. In the study, we assumed  $\nu$  to be 0.4999 in all simulations.

The mathematical equations were solved numerically, using a finite element method (COMSOL software, version 4.4).

The simulations were divided into two groups. In the first one, indentation of a semi-finite half space was investigated for the validation of **Equation 2**. The half space was modeled as a cubic block with size of  $H$  (see **Figure S1**); and the spherical tip of the AFM probe was placed at the center of the top surface. Due to the geometric symmetries in the  $x$ - and  $y$ -directions, only a quarter of the block needs to be considered in the simulations. For given values of  $E_0$ ,  $H$ , and a set of values of indentation ( $\delta$ ), ranging from  $0$  to  $R/2$ , the indentation force ( $F$ ) was solved as a function of  $\delta/R$ . The simulated  $F$  vs.  $\delta/R$  profiles were fitted with **Equation 2** to obtain the value of  $(E_0)_{app}$ . The relative difference between  $E_0$  and  $(E_0)_{app}$  was used as a measure of error in the initial Young's modulus determined by **Equation 2**. It was observed that  $R^2$  was 1.00 in all regression analyses, and that the error decreased with increasing  $H$ , the size of the cube (see **Table S1**). The error was independent of  $E_0$  since  $F$  was proportional to  $E_0$ . The simulation converged when  $H > 150 \mu\text{m}$ . At  $H = 175 \mu\text{m}$ , the error for the estimated  $E_0$  was 0.02%.

Results from simulations in the second group were used to evaluate errors in the estimated  $E_0$ , i.e.,  $(E_0)_{app}$ , caused by structural heterogeneity in ocular tissues. As mentioned above, **Equation 2** was derived for analysis of AFM indentation of a homogenous semi-finite half space, whereas ocular tissues consist of TM, cornea, sclera, and other structures. And each of them has finite dimensions. Additionally, the exact location of the borders between TM and surrounding tissues were unknown in our experiments. They could only be estimated, based on Evans blue and pigment distributions in tissues. To evaluate how the finite tissue size and the uncertainty in the TM location affected  $(E_0)_{app}$ , we developed a mathematical model to numerically simulate ocular tissue indentation. To simplify the model, we assumed that TM, cornea, and uveosclera were incompressible, isotropic, and homogeneous neo-Hookean materials with different initial Young's moduli ( $E_0$ ). The model geometry was constructed based on the histology section of rat eyes (see **Figure 3**). The curvatures of SC and TM were neglected because they were significantly smaller than the dimensions of the cross sections of both SC and TM. As a result, all tissues in our model were assumed to be straight cylinders with different shapes of cross-sections. **Figure S2** shows the cross-section through the center of the AFM tip. Due to the geometric symmetry in the  $y$ -direction, only half of the volume was considered in

numerical simulations. The half-width of the volume in the y-direction (i.e., the half-length of the cylinders) is  $L_0$ ; and other dimensions (i.e.,  $H_1$ ,  $L_1$ , and  $L_2$ ) of the volume are indicated in **Figure S2**. The volume size had insignificant effects on simulation results if each dimension was greater than  $100\ \mu\text{m}$  as indicated in our pilot simulations (data not shown). Thus,  $L_0$ ,  $H_1$ ,  $L_1$ , and  $L_2$  were all assumed to be  $100\ \mu\text{m}$ . To derive boundary conditions, we assumed that the displacement of the bottom surfaces of both sclera and cornea (i.e.,  $z = -100\ \mu\text{m}$ ) was zero. At other boundaries, the stresses were zero except at the area of contact between ocular tissue and the spherical tip of AFM probe, where continuous displacement and stresses were assumed. The total force exerted on the tip is  $F$ . The value of  $E_\theta$  was tissue-dependent, which was chosen to be 160 Pa, 2000 Pa, and 6200 Pa for TM, sclera, and cornea, respectively. They were approximately equal to the geometric means of the experimental data of  $(E_\theta)_{app}$  in Regions 1, 3, and 5, respectively (see **Table 3**). The simulations were repeated for indentation at different locations indicated by  $x_0$ , i.e., the x coordinate of the center of the spherical tip, which varied from  $-40$  to  $140\ \mu\text{m}$ . In addition to the  $F$  vs.  $\delta/R$  profiles, we calculated three-dimensional distributions of the total displacement in tissues.

To simulate effects of partial detachment of TM from the cornea on  $(E_\theta)_{app}$ , we modified the model geometry by cutting out a rectangular region in the cornea (see **Figure S3**). The dimensions of the region in x-, y-, and z-directions are  $25\ \mu\text{m}$ ,  $100\ \mu\text{m}$  (i.e.,  $L_0$ ), and  $8\ \mu\text{m}$ , respectively. The procedure of the simulation was the same as that for the intact TM. The simulated  $F$  vs.  $\delta/R$  profiles were fitted with **Equation 2** to determine the apparent Young's modulus of the partial detached TM,  $(E_\theta)_{det}$ .

**Table S1: Comparison of  $E_0$  and  $(E_0)_{app}$  for Simulated Indentation of a Uniform Cube <sup>†</sup>**

Cube height, $H$ ( $\mu\text{m}$ )	$(E_0)_{app}/E_0$	Percent difference
25	1.0994	9.94%
50	1.0406	4.06%
75	1.0212	2.12%
100	1.0119	1.18%
125	1.0055	0.54%
150	1.0022	0.22%
175	0.9998	0.02%
200	1.0004	0.04%

<sup>†</sup> Indentation of a uniform cube was simulated numerically. For given values of  $E_0$  and  $H$ , the indentation force ( $F$ ) was simulated as a function of  $\delta/R$ , where  $\delta$  is the indentation and  $R$  is the tip radius of AFM probe. The simulated  $F$  vs.  $\delta/R$  curves were fitted with **Equation 2** to yield the values of apparent initial Young's modulus,  $(E_0)_{app}$ . The ratio and percent difference between  $E_0$  and  $(E_0)_{app}$  were independent of  $E_0$  when its value was varied from 100 to 7000 Pa.

## References

1. D. C. Lin, E. K. Dimitriadis and F. Horkay, *Express Polym Lett*, 2007, **1**, 576-584.
2. D. C. Lin, D. I. Shreiber, E. K. Dimitriadis and F. Horkay, *Biomechanics and modeling in mechanobiology*, 2009, **8**, 345-358.
3. R. Long, M. S. Hall, M. Wu and C. Y. Hui, *Biophysical journal*, 2011, **101**, 643-650.
4. X. Xu, A. Jagota and C. Y. Hui, *Soft matter*, 2014, **10**, 4625-4632.
5. H. Y. Yu, S. C. Sanday and B. B. Rath, *J Mech Phys Solids*, 1990, **38**, 745-764.

## Figure legend

- Figure S1.** Indentation of a semi-finite half space. The half space was modeled as a cubic block of neo-Hookean material. The indentation occurred at the center of the top surface. The tip size of AFM probe and the indentation force ( $F$ ) are indicated in the figure. The size  $H$  varied from 25 to 200  $\mu\text{m}$  in the simulations.
- Figure S2.** Schematic of the model geometry for numerical simulations of ocular tissue indentation. TM, uveosclera, and cornea were modeled as cylindered with different shapes of cross-sections. The tip of AFM probe was spherical. The x- and z-axes are shown in the figure, and the y-axis is in the direction determined by the right-hand rule. The indentation of ocular tissues was caused by a force ( $F$ ) exerted on the tip of AFM probe; and the tissue deformation was symmetric about the plane of  $y = 0$ . All dimensions in the x- and z-directions are indicated in the figure. The half-width of the volume in the y-direction (i.e., the half-length of the cylinders) was  $L_0$ .
- Figure S3.** Schematic of the model geometry for numerical simulations of indentation of ocular tissues with partial detachment of the TM. It is the same as the geometry shown in Figure S2, except that a rectangular region of the cornea was removed to model the partial detachment of the TM. The dimensions of the region in x- and z-directions are shown in the figure. In the y-direction, it is  $L_0$ .

Figure S1

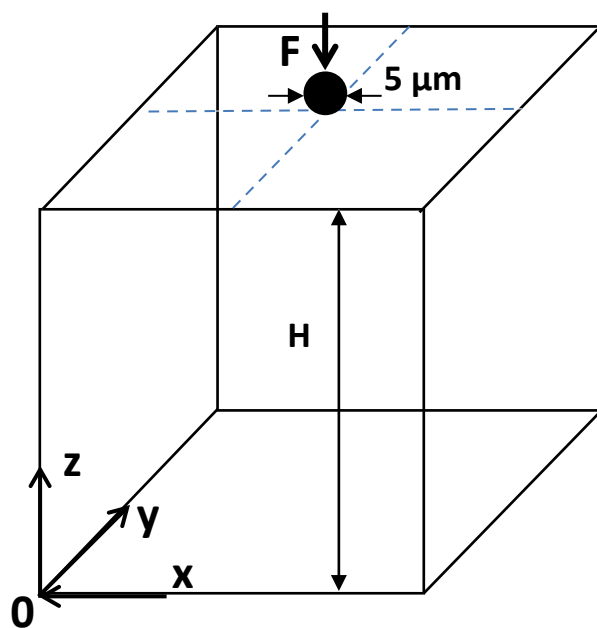


Figure S2

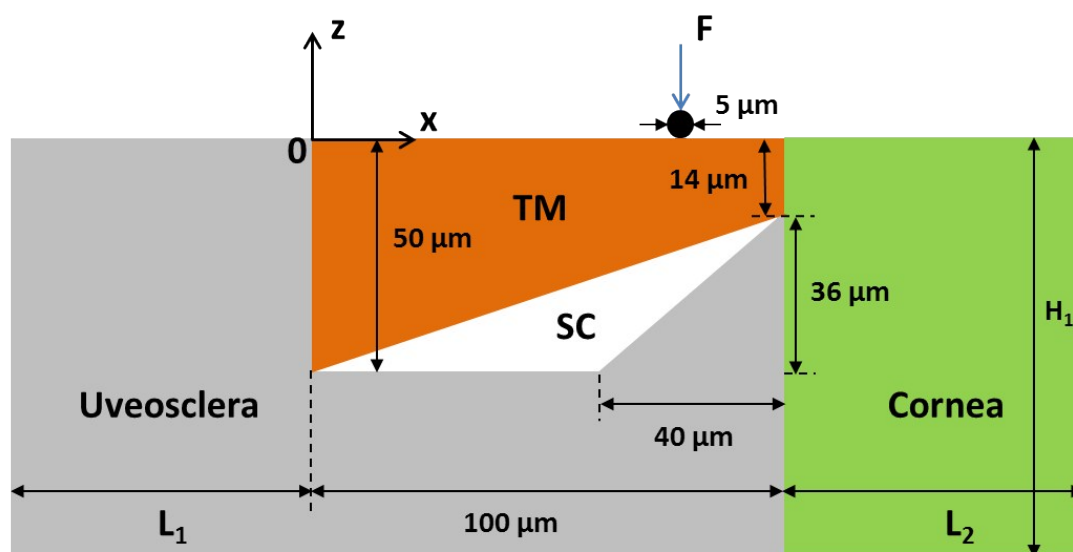


Figure S3

